Journal of Modern Optics
Publication details, including instructions for authors and subscription information:
http://www.tandfonline.com/loi/tmop20

Apodized distributed feedback fiber laser as an optical filter

Nazmi A. Mohammed[a], Ayman W. Elashmawy[a] & Moustafa H. Aly[a]
[a] Department of Electronics and Communications, Arab Academy for Science, Technology and Maritime Transport, Alexandria, Egypt
Published online: 13 Nov 2013.

To cite this article: Nazmi A. Mohammed, Ayman W. Elashmawy & Moustafa H. Aly , Journal of Modern Optics (2013): Apodized distributed feedback fiber laser as an optical filter, Journal of Modern Optics, DOI: 10.1080/09500340.2013.853847

To link to this article: http://dx.doi.org/10.1080/09500340.2013.853847

Journal of Modern Optics, 2013
http://dx.doi.org/10.1080/09500340.2013.853847

Taylor & Francis
Taylor & Francis Group

Apodized distributed feedback fiber laser as an optical filter

Nazmi A. Mohammed, Ayman W. Elashmawy* and Moustafa H. Aly

Department of Electronics and Communications, Arab Academy for Science, Technology and Maritime Transport, Alexandria, Egypt

(*Received 25 June 2013; accepted 30 September 2013*)

The potential was investigated of using distributed feedback fiber lasers (DFB-FLs) with different apodizations for C-band optical filtering. Design optimizations were carried out, to mainly target ultra-dense wavelength division multiplexing (UDWDM) filtering specifications. Optimization led to choice of the positive-tanh apodization profile as being the most suitable for UDWDM filtering specifications.

Keywords: distributed feedback fiber laser; fiber Bragg grating; ultra-dense wavelength division multiplexing; apodization profile; optical filter

1. Introduction

Signal processing in the optical domain is considered a promising technique for many applications such as radar and broadband wireless access networks. Use of the high-frequency processing capability and wide-band signals directly in the optical domain avoids the need for inefficient and costly intermediate conversions to and from the optical and electrical domains. This makes it convenient in a number of frequency and time domain applications, such as filtering, correlation, and Fourier transformation [1].

Spectrally tunable optical filters are of interest for a wide variety of applications including pulse shaping, pulse rate multiplication, optical code-division multiple-access (OCDMA), and dispersion compensation. Also, they can be used in fiber laser systems and wavelength division multiplexing (WDM) techniques with multiple channels [2].

Different filter configurations have been proposed such as optical couplers, Mach–Zehnder lattices, high dispersion fibers, arrayed waveguide gratings (AWGs), or fiber Bragg gratings (FBGs), which can be used as the main elements. Among these elements, FBGs have the advantages of a simple structure, low insertion loss, high wavelength selectivity, polarization insensitivity, and full compatibility with single mode optical fibers [3–5].

An FBG features a periodic or non-periodic perturbation of the effective refractive index in the core; it is periodic over a certain length of a few millimeters. There are various structures of FBGs, such uniform, apodized, chirped, tilted, and long period. When light propagates through an FBG, the total reflection takes place at the Bragg wavelength and other wavelengths are not affected by the Bragg grating; however, some side lobes exist in the reflection spectrum. These side lobes can be suppressed using apodization techniques and the reflection spectrum depends on the length and strength of the refractive index modulation [6].

Tunable FBG filters have been designed and become good solutions for creating dynamic optical systems [7]. This is usually motivated by the WDM system requirements, which can also be dense (DWDM) or ultra-dense (UDWDM). In order to obtain good filter performance, FBGs must have the following spectral characteristics [8–10]:

- A narrow full width at half maximum (FWHM) to give the ability to accord spacing wavelength.
- Weak side lobe peaks to avoid bandwidth (BW) overlapping (i.e. to obtain a high side lobe suppression ratio [SLSR]).
- The filter must be able to tune wavelengths in the WDM (0.8–1.6 nm wavelengths spacing), DWDM (0.2–0.4 nm wavelengths spacing), and UDWDM (wavelength spacing <0.2 nm) windows.
- The temperature or strain tuned response should not affect the width of the BW nor the amplitude of the reflection peak.

Periodic fiber gratings with constant refractive index modulation depths (i.e. un-apodized) show reflection spectra with large side lobes, as well as highly nonlinear dispersion characteristics which make them unsuitable for high-performance applications. These characteristics are attributed to residual multiple reflections at the grating ends and can be significantly suppressed by a suitable variation (apodization) of the modulation depth along its length. The reflection spectrum of an apodized,

*Corresponding author. Email: a_elashmawy@hotmail.com

periodic standard grating closely follows the Fourier transform of the applied apodization profile. As a result, smooth and tight apodization profiles result in enhanced side-lobe suppression and superior grating performance [11,12].

Distributed feedback fiber lasers (DFB-FLs) possess certain unique properties that make them attractive for a number of different applications. They are inherently fiber compatible, need a very simple passive thermal stabilization to ensure the stability of the laser, provide high output power (up to 60 mW), single frequency, single polarization, and high optical signal-to-noise ratio (OSNR) [13].

DFB-FLs have been widely used in sensing and communication systems, as well as high-precision spectroscopy; all of which require single-mode and single-frequency lasers [14,15].

The DFB-FL is similar to the FBG, but with a gain applied to the grating section; this means that the DFB-FL gives the same response of the FBG when the gain is set to zero [16].

This work investigated the potential of using DFB-FLs as optical filters by applying different apodization functions. A parametric study was applied for all apodization functions to optimize the filter performance to match UDWDM–WDM filtering specifications and judge their responses. Finally, a comparison between different apodized DFB-FL filters, as well as DFB-FL filters and well-known apodized FBG filters is carried out.

This paper is organized as follows: in Section 2, we present the proposed structure of the DFB-FL and the mathematical model upon which simulations will be based and introduce the apodization functions used in this paper. The results of simulations for various grating lengths and different refractive index variations are reported and discussed in Section 3. Finally, we summarize and conclude the results obtained in Section 4.

2. Mathematical model

2.1. DFB-FL coupled mode equations

Coupled mode theory [17] is used to analyze the threshold behavior in simple DFB lasers. Figure 1 shows forward and backward waves in waveguides induced by periodic modulation of the refractive index n.

For a uniform DFB-FL, the coupled-wave equations can be written as [18]:

Figure 1. Forward and backward waves in periodic active waveguides.

$$\frac{dR(z)}{dz} = \left(g - j\delta + \frac{1}{2}\frac{d\phi(z)}{dz}\right)R(z) - j\kappa S(z), \tag{1a}$$

$$\frac{dS(z)}{dz} = -\left(g - j\delta + \frac{1}{2}\frac{d\phi(z)}{dz}\right)S(z) + j\kappa R(z), \tag{1b}$$

$$\delta = \beta - \beta_D = 2\pi n_{eff}\left(\frac{1}{\lambda} - \frac{1}{\lambda_D}\right), \tag{2}$$

$$\kappa = \frac{\pi}{\lambda} n_a f_A\,(z), \tag{3}$$

where g is the gain of the DFB active region per unit length, δ is the detuning of the propagation constant from the Bragg condition, n_{eff} is the effective refractive index of the fiber core, λ is the wavelength of the incoming signal, λ_D is the design filter wavelength, κ is the coupling coefficient between the forward and backward waves, $\phi(z)$ is the wave phase, n_o is the maximum modulation amplitude of the refractive index (modulation depth), and $f_A(z)$ is the apodization profile function.

In analysis, it is assumed that there is no grating chirp, i.e. $[d\phi/dz = 0]$, and that the gain is given by $g = 0.98g_{th}$ as in the case of the uniform DFB-FL to avoid lasing behavior of the DFB-FL and to operate as an optical filter [18], where g_{th} is the threshold gain given by [19]

$$g_{th} = 4\kappa_m e^{-\kappa_m L} + \alpha_s, \tag{4}$$

$$\kappa_m = \frac{\pi}{\lambda} n_o, \tag{5}$$

where L is the grating length of the amplifier, κ_m is the maximum value of the coupling coefficient in a uniform DFB-FL, so the threshold gain varies according to L, n_o, and α_s, which is the background loss of the used fiber.

Equations (1) can be merged into a single equation by defining $u(z) = S(z)/R(z)$ and differentiating with respect to z, resulting in

$$\frac{du(z)}{dz} + 2(g - j\delta)u(z) - j\kappa(1 + u^2(z)) = 0, \tag{6}$$

where the boundary condition is $u(L) = 0$, representing the situation in which no backward wave is incident from the other side. Now, Equation (6) can be solved to obtain the reflection coefficient (r) at the input, i.e. $u(0) = S(0)/R(0)$, as such obtaining the reflectivity = $|r|^2$. The DFB-FL can be converted to a FBG structure when setting zero gain, as will be explained in the next section.

2.2. Effect of gain on reflectivity spectrum and FWHM for uniform DFB-FL

In this section, the effect of gain on the reflectivity spectrum and FWHM for a uniform DFB-FL structure is explored from no gain to lasing.

Figure 2 presents a comparison between only uniform DFB-FL and uniform FBG (DFB-FL with no gain) with a grating length and modulation depth of 15 mm and 10^{-4}, respectively. As shown in Figure 2, the FBG's peak reflectivity is near unity as there is no gain, while the DFB-FL's peak reflectivity is very large as the device is near oscillation. The FWHM of the FBG is about 0.134 nm, while that of the DFB-FL is about 2 pm, which makes the DFB-FL preferable in optical filtering applications due to high selectivity.

Also, as shown in Figure 2, the FBG exhibits large side lobes, making the SLSR as low as 5 dB. On the other hand, the DFB-FL has nearly no side lobes making it better for operation as a filter; however, the only disadvantage of using the DFB-FL is the existence of two peaks. This should be solved to have single wavelength filtering.

Figure 3 presents the effect of varying the gain as a free parameter on the reflectivity spectrum for the uniform DFB-FL structure starting from no gain to lasing at same design values (L, n_o) as in Figure 2. As shown in Figure 3, it is clear that increasing the gain converts the well-known FBG reflectivity spectrum to the DFB-FL reflectivity spectrum. The DFB-FL spectrum (splitting of the spectrum into two peaks) is observed for higher gain values ($g \geq 0.5g_{th}$). Highly selective lasing wavelengths are observed when the gain approaches the threshold value. This selectivity feature is promising for optical filtering applications.

Figure 4 shows the effect of gain variation from no gain to lasing on the FWHM for a uniform DFB-FL under same design values (L, n_o) used in Figures 2 and 3. As shown in Figure 4, at small gain values below $0.5g_{th}$, the bandwidth is relatively wide and the well known FBG reflectivity spectrum is observed. As the gain increases above $0.5g_{th}$, the spectrum begins to split, as described above. This leads to narrowing of the bandwidth for every split spectrum and to a rapid decrease the FWHM, making it suitable for high selective filtering applications.

Based on the previous explanations, this work introduces different apodization profiles on DFB-FLs to provide single band filtering suitable for remarkable UDWDM filtering performance. This work aims to achieve higher reflectivity, a more selective filter having a small FWHM, negligible or no side lobes, smoother response, and a smaller transition interval.

2.3. *Apodization profiles*

The main apodization profiles, considered in the present investigation, are [20–22]:

(1) Positive-tanh profile:

$$f_A(z) = \begin{cases} \tanh\left(\dfrac{2az}{L}\right), & 0 \leqslant z \leqslant \frac{L}{2} \\ \tanh\left(\dfrac{2a(L-z)}{L}\right), & \frac{L}{2} \leqslant z \leqslant L \end{cases}$$

(2) Gaussian profile:

$$f_A(z) = \exp\left(-G\left(\frac{z-\frac{L}{2}}{L}\right)^2\right), \quad 0 \leqslant z \leqslant L$$

(3) Hamming profile:

$$f_A(z) = \frac{1 + H\cos\left(\dfrac{2\pi(z-\frac{L}{2})}{L}\right)}{1+H}, \quad 0 \leqslant z \leqslant L$$

(4) Cauchy profile:

$$f_A(z) = \frac{1-\left(2\left(\dfrac{z-\frac{L}{2}}{L}\right)\right)^2}{1-\left(2C\left(\dfrac{z-\frac{L}{2}}{L}\right)\right)^2}, \quad 0 \leqslant z \leqslant L$$

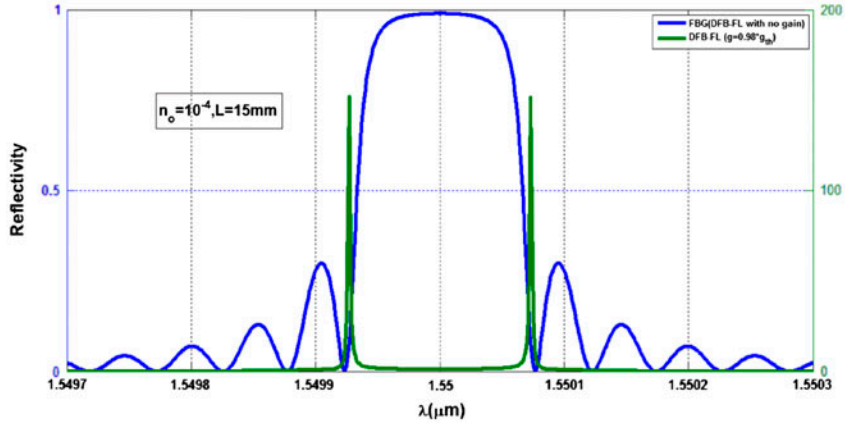

Figure 2. Reflection spectra for uniform DFB-FL and uniform FBG. (The color version of this figure is included in the online version of the journal.)

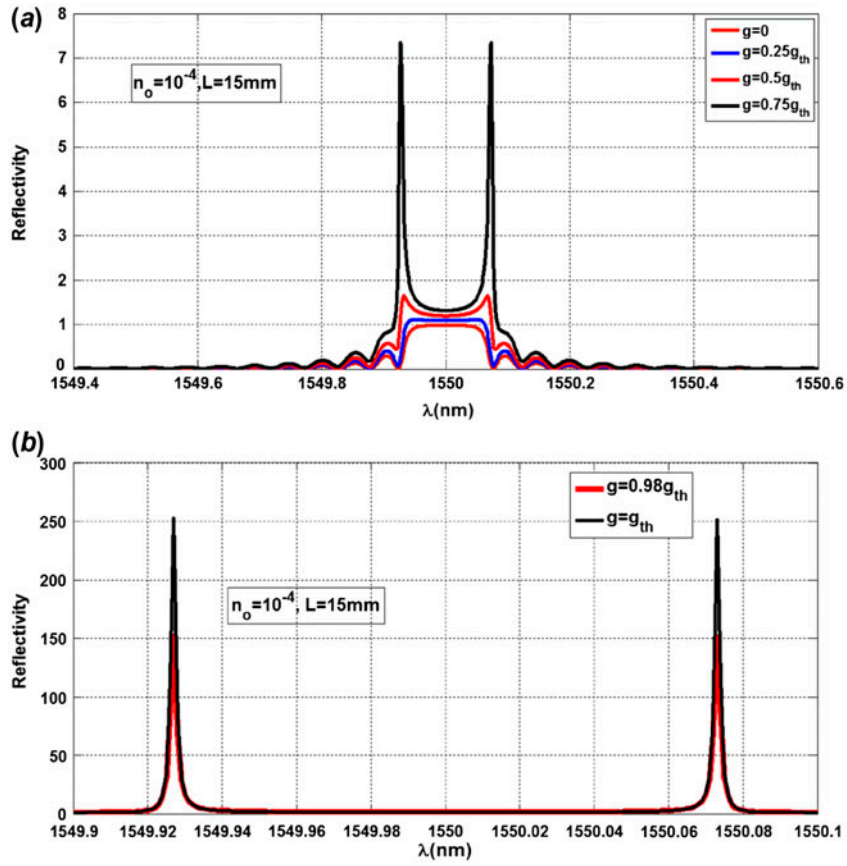

Figure 3. Reflectivity spectrum for uniform DFB-FL at variable gain. (The color version of this figure is included in the online version of the journal.)

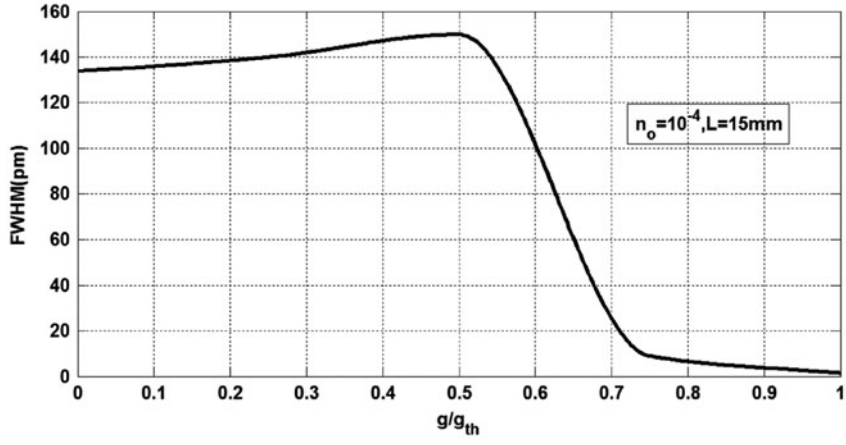

Figure 4. FWHM variations with gain for uniform DFB-FL.

In the above, a is the positive-tanh parameter, G is the Gaussian parameter, H is the Hamming parameter, and C is the Cauchy parameter.

The apodization profiles applied to the DFB-FL are shown in Figure 5. The positive-tanh profile (a = 4) [16] has a flat region that allows strong coupling between the forward and backward waves in the grating region. The Cauchy profile (C = 0.5) [23] has a wide profile that can allow a good interaction between waves. For the Hamming profile (H = 0.665) [22], the profile varies with a

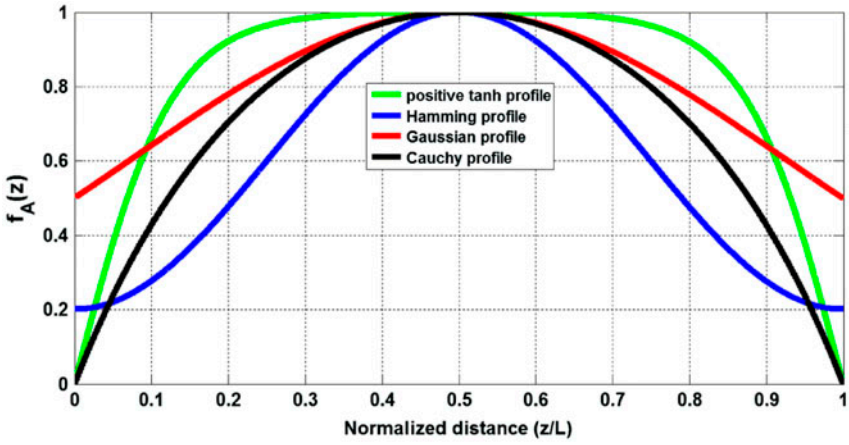

Figure 5. Apodization profiles for DFB-FL. (The color version of this figure is included in the online version of the journal.)

steep transition that does not reach zero. The Gaussian profile (G = 4ln 2) [21] has a variation between half and unity.

2.4. Runge–Kutta fourth order method

Equation (6) cannot be solved exactly, so the Runge–Kutta fourth order method (RKM4) was used to solve it numerically. The initial boundary condition is u_{intial}, varying the iterations with step (h) so one can reach the desired point u_{final} [24].

3. Results and discussion

3.1. Introduction

For every apodization profile, the coupling coefficient (κ) is changed according to Equation (3). The coupling coefficient and Equation (2) are substituted in Equation (6) and the RKM4 used to solve it numerically. The solution, together with what was mentioned in Section 2.1, is used to calculate the reflectivity.

In the following sections, the reflectivity spectrum is evaluated for different apodization profiles in the DFB-FL filter. This evaluation is associated with a detailed study of the effect of grating length (L) and the maximum modulation of refractive index (n_o).

For each apodized DFB-FL filter design, optimum values of L and n_o are chosen to satisfy the specifications of the optical filter. The parameters used in simulations are a_s = 0.15 m^{-1}, n_{eff} = 1.47 [19]. The grating length varies from 5 mm to 30 mm [25], n_o varies from low modulation depth (10^{-5}) to large modulation depth (10^{-3}) [21]. The wavelength simulation range is chosen to cover effective parts of the C-band that are suitable for filtering operation and do not cause lasing behavior, as observed from simulations. Previous choices provide the ability to compare with previous literature results. Finally, the performance of different apodized DFB-FL filters is compared with that of well-known apodized FBG filters.

3.2. Positive-tanh apodized DFB-FL as an optical filter

Figure 6 shows the reflectivity wavelength spectrum with changing grating length at constant modulation depth ($n_o = 10^{-5}$) for the positive-tanh apodization profile. The unclear spectra observed at L = 5 mm and 1mm are presented more clearly as insets of Figure 6. As shown in Figure 6, the reflectivity increases with length, while the FWHM decreases. There is a small side lobe at smaller lengths and suppressed side lobe for L $\geqslant$ 15 mm and the reflectivity spectrum differs in the transition from the pass band to the stop band. For wavelengths near the center designed wavelength λ_D (i.e. $\delta \sim 0$) and sufficiently high gain, as in the cases of L = 30 mm and 25 mm, the condition of oscillation is nearly satisfied, allowing the device to exhibit high gain so reflectivity increases beyond 1.

For optimum filter design the target is high reflectivity, narrow FWHM, and a suppressed side lobe; a tradeoff between these three parameters should be made. Optimization leads to the choice of L = 25 mm as it provides a peak reflectivity of 1.906, a FWHM of about 0.048 nm, and no side lobes, making it suitable for UDWDM filter applications, as stated in Section 1.

Figure 7 shows the reflectivity spectrum against the maximum refractive index amplitude, at L = 25 mm. As shown in Figure 7, by increasing n_o the reflectivity increases resulting in a wider spectrum; thus the FWHM increases and there are side lobes for moderate modulation depth ($n_o = 10^{-4}$).

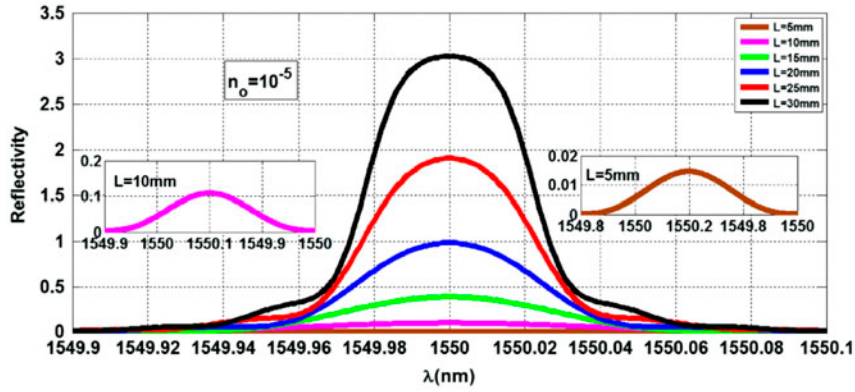

Figure 6. Reflectivity of positive-tanh apodization profile at $n_o = 10^{-5}$. (The color version of this figure is included in the online version of the journal.)

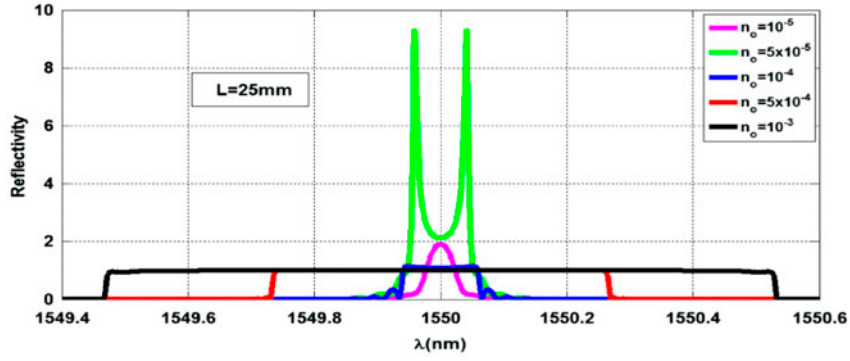

Figure 7. Reflectivity of positive-tanh apodization profile at $L = 25$ mm. (The color version of this figure is included in the online version of the journal.)

For $n_o = 5 \times 10^{-5}$, the reflectivity shows two peaks for two different wavelengths achieved near the oscillation condition. The optimum case is $n_o = 10^{-5}$ which provides a peak reflectivity, a FWHM that is previously obtained, and no side lobes, in addition to a steep transition.

The optimization procedure using this apodization was aimed at targeting UDWDM filter operation and led to the previously chosen values for L and n_o. If we target less selective filters (only WDM filter applications, wider FWHM), the modulation depth of the grating must be increased to $n_o = 10^{-3}$ giving a SLSR of 22.3 dB, a wider FWHM (1.06 nm), and a reflectivity which is nearly 1. As shown in Figure 7, this can be used as a very good optical band pass filter. This dual filter operation behavior is available using this apodization and the Cauchy profile, as will be discussed in Section 3.5.

3.3. *Hamming apodized DFB-FL as an optical filter*

The reflectivity spectrum under grating length variation for constant modulation depth ($n_o = 10^{-5}$) is shown in Figure 8 for the Hamming apodization profile. The unclear spectra observed at $L = 5$ mm and 10 mm are presented more clearly as insets of Figure 8. As is shown, increasing L with fixed n_o causes the reflectivity to decrease, the FWHM to decrease, and a steep transition to appear from the pass band to the stop band. Also, the main lobe is wide for small lengths and no side lobes appear. The optimum case is when $L = 30$ mm, providing a peak reflectivity of 1.883, a FWHM of 0.04 nm, and no side lobes; this can be used in UDWDM filter applications. There is a notch which is 1.59% of the maximum at center wavelength due to the apodization profile.

Figure 9 shows the spectrum of the reflectivity against the maximum modulation refractive index amplitude for constant grating length ($L = 30$ mm). As shown in Figure 9, side lobes appear for $n_o \geq 5 \times 10^{-5}$, causing degradation in SLSR while the FWHM increases. The spectrum is not flat at $n_o = 10^{-3}$, which makes it unsuitable for wider bandwidth filters; for wider filters, the most suitable design is at $n_o = 5 \times 10^{-4}$. The optimum values for selective filters are obtained at $n_o = 10^{-5}$ providing the reflectivity and FWHM previously obtained with no side lobes.

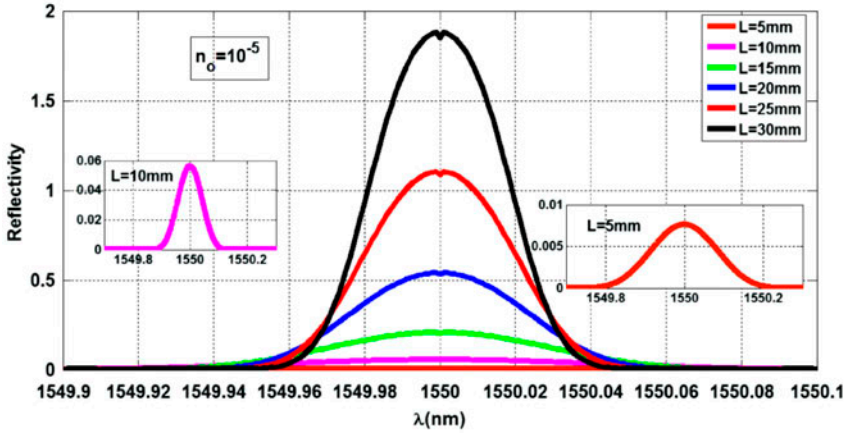

Figure 8. Reflectivity of Hamming apodization profile at $n_o = 10^{-5}$. (The color version of this figure is included in the online version of the journal.)

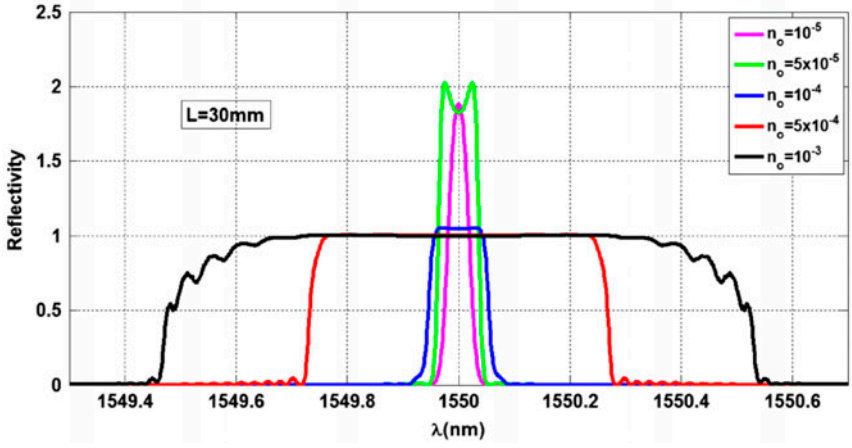

Figure 9. Reflectivity of Hamming apodization profile at $L = 30$ mm. (The color version of this figure is included in the online version of the journal.)

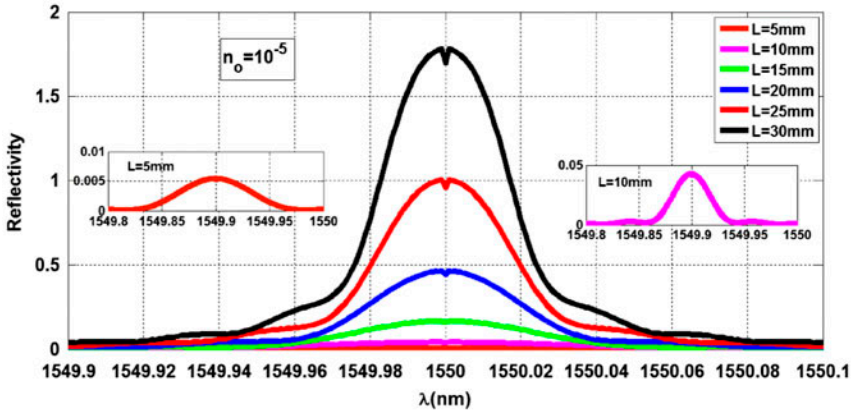

Figure 10. Reflectivity of Gaussian apodization profile at $n_o = 10^{-5}$. (The color version of this figure is included in the online version of the journal.)

3.4. Gaussian apodized DFB-FL as an optical filter

Figure 10 shows the reflectivity spectrum at different grating lengths for $n_o = 10^{-5}$ for a Gaussian apodization profile. The unclear spectra observed at $L = 5$ mm and 10 mm are presented more clearly as insets of Figure 10. As L increases, reflectivity increases, the FWHM decreases, and side lobes begin to decrease; however, the main lobe is spread over a wider range of wavelengths, as shown in Figure 10. The best case is at $L = 20$ mm, providing a peak reflectivity of 0.4666, a FWHM of 0.046 nm, and a SLSR of 10.62 dB.

Just like the Hamming profile, the Gaussian apodization profile exhibits a high gain for $L = 30$ mm and a notch which is 4.42% of the maximum at center wavelength, as shown in Figure 10. Figure 11 shows the reflectivity wavelength spectrum as a function of n_o at optimum length ($L = 20$mm). The amplification property appears at $n_o = 5 \times 10^{-5}$ but the spectrum exhibits two peaks in the pass band, as a result degrading single wavelength filtering performance. High side lobes appear for high modulation depth, causing SLSR degradation and an increase in FWHM, as shown in Figure 11.

For the best case, the maximum amplitude modulation is chosen to be 10^{-5} to obtain the above results for reflectivity, FWHM, and SLSR.

3.5. Cauchy apodized DFB-FL as an optical filter

The reflectivity spectrum under variation of grating length at $n_o = 10^{-5}$ is shown in Figure 12 for a Cauchy apodization profile; the unclear spectrum observed at L = 5 mm is presented more clearly as an inset of the figure. From Figure 12, the reflectivity increases with length, the FWHM decreases, and side lobes are suppressed with a negligible notch (0.1% of maximum). For the optimum case, the choice will be $L = 20$ mm, providing a peak reflectivity of 0.7303, FWHM of about 0.054 nm, and no side lobes.

The corresponding reflectivity wavelength spectrum under n_o variation for $L = 20$ mm is shown in Figure 13. As can be seen, the response of the Cauchy profile is similar to the positive-tanh profile with two peaks at $n_o = 5 \times 10^{-5}$. Optimization leads to choice of $n_o = 10^{-5}$, which provides the reflectivity, FWHM, and suppressed side lobes previously obtained.

3.6. Comparison

3.6.1. Comparison between apodized DFB-FL filter designs

Table 1 compares the performance of the different apodization profiles. The positive-tanh profile is smooth, showing no notches in the pass band, the Cauchy profile has a negligible notch (0.1% of the maximum) compared to the Hamming and Gaussian apodization profiles that have a notch at the central wavelength. The notch is about 1.53% for the Hamming profile and 4.42% for the Gaussian profile; this makes positive-tanh and Cauchy profiles a good choice when considering only the filter shape response.

Gaussian and Cauchy apodization profiles require a small grating length (20 mm), the positive-tanh requires a larger length (25 mm), while Hamming profile requires the largest grating length (30 mm). As for the modulation depth, all the apodization profiles require small modulation depth (10^{-5}).

The high gain property depends on the apodization profile as it appears in positive-tanh and Hamming profiles but the gain is not high enough for other apodization profiles to come close to achieving the oscillation condition so their reflectivities are less than 1 and they need a larger length to achieve it.

Considering FWHM, the positive-tanh, Hamming, and Gaussian profiles give a nearly equal FWHM while the Cauchy profile is slightly larger. Considering side lobes, there are large side lobes in the Gaussian profile, while

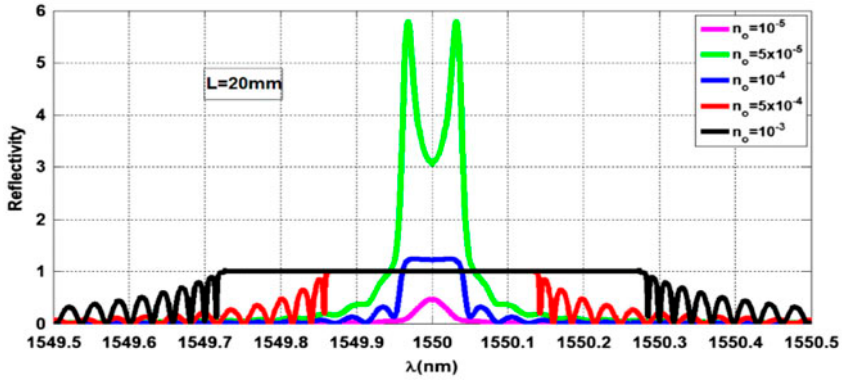

Figure 11. Reflectivity of Gaussian apodization profile at $L = 20$ mm. (The color version of this figure is included in the online version of the journal.)

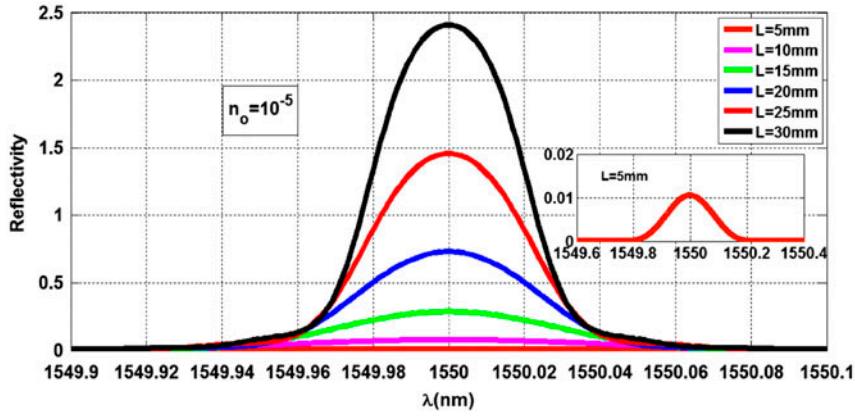

Figure 12. Reflectivity of Cauchy apodization profile at $n_o = 10^{-5}$. (The color version of this figure is included in the online version of the journal.)

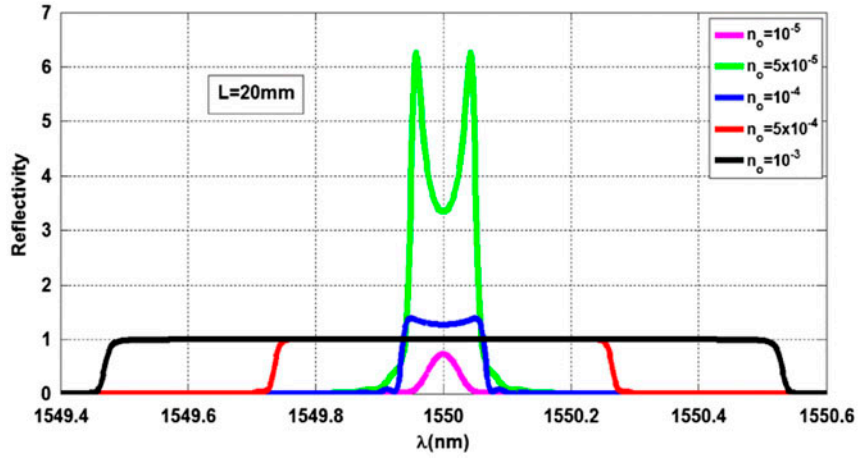

Figure 13. Reflectivity of Cauchy apodization profile at $L = 20$ mm. (The color version of this figure is included in the online version of the journal.)

Table 1. Summary of apodization profile results.

Apodization profile	L (mm)	n_o	Peak reflectivity	FWHM (nm)	SLSR (dB)	Notches
Positive-tanh	25	10^{-5}	1.906	0.048	–	No
Hamming	30	10^{-5}	1.883	0.04	–	1.53%
Gaussian	20	10^{-5}	0.4666	0.046	10.62	4.42%
Cauchy	20	10^{-5}	0.7303	0.054	–	0.1%

they are suppressed in the case of positive-tanh and Hamming profiles; negligible side lobes are present in Cauchy profile, making the latter three the better filters.

Out of previous filter design specifications that target UDWDM filter applications, increasing the modulation depth in positive-tanh, Cauchy, and Hamming apodization profiles leads to widening of the reflectivity spectrum curve and increasing the FWHM for the filter, making them suitable for wider WDM filter applications; however, in the Gaussian profile the side lobes rapidly increase, degrading the filter performance.

Figure 5 shows the apodization profiles used in designing DFB-FLs to provide suitable filtering performance. From Sections 3.3 and 3.4, dips at 1550 nm are observed in Hamming and Gaussian reflectivity spectra under parameters used in Figure 5. Simulation results show that this behavior is due to the chosen $H = 0.665$ and G = 4ln 2 that are set in Figure 5 to provide a better filtering performance. However, these dips can be

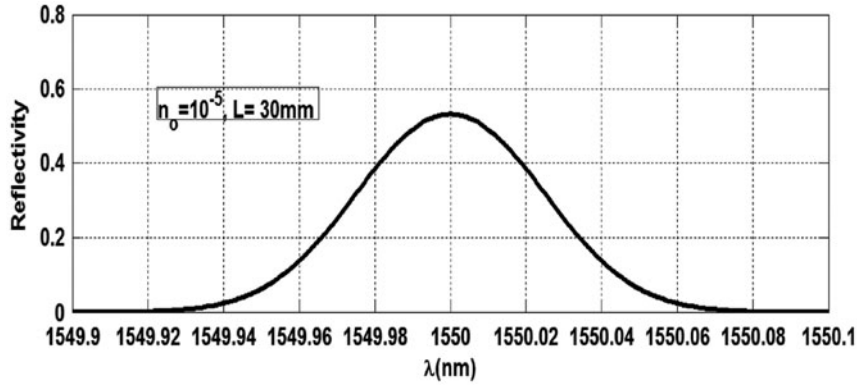

Figure 14. Reflectivity spectrum for Gaussian profile (G = 30).

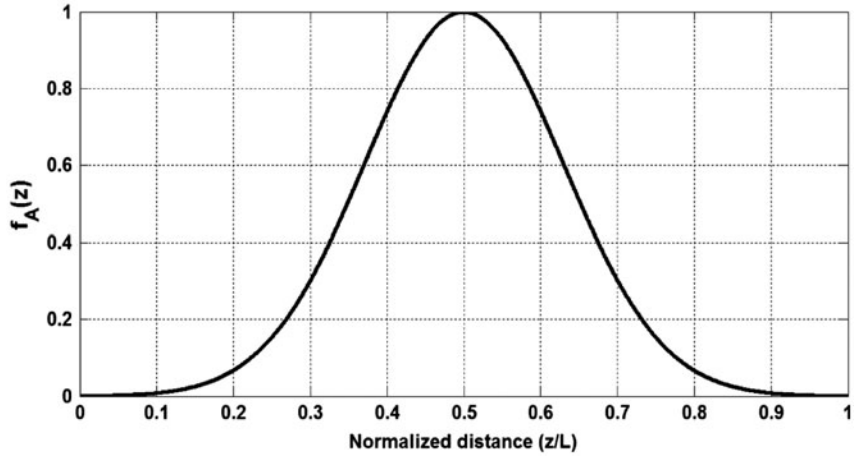

Figure 15. Gaussian profile with G = 30.

removed by adjusting H and G parameters to provide lower quality filter (i.e. the peak reflectivity will be reduced and the FWHM will be wider).

As an explanation for the previous point, Figure 14 presents the reflectivity spectrum of the DFB-FL without dips at 1550 nm for the Gaussian profile with G = 30, L = 30 mm, and n_o = 10^{-5}. This reflectivity spectrum is associated with the apodization profile with G = 30 shown in Figure 15.

As observed from Figures 10 and 14, the peak reflectivity decreases from 1.782 to 0.532 and the FWHM is increased from 0.038 nm to 0.058 nm, resulting in a less selective optical filter.

3.6.2. *Comparison of apodized DFB-FLs with apodized FBGs*

Table 2 shows the features of some well-known profiles for apodized FBGs that are used as filters [16,21,22,25,26,28,29].

As shown in Tables 1 and 2, the DFB-FL positive-tanh profile needs a smaller grating length compared to the FBG positive-tanh profile of the same modulation depth (10^{-5}), giving a narrower FWHM and higher peak reflectivity. It gives better performance than the positive-tanh FBG profile due to the weaker modulation depth, compact (small) length, higher reflectivity, and suppressed side lobes that make it better for more selective filters.

For the Hamming profile, compared to the FBG the DFB-FL needs a shorter grating length and weaker modulation depth to obtain an acceptable narrow FWHM (0.04 nm), higher peak reflectivity (1.883), and no side lobes, resulting in a more compact size and better design which is made easier to fabricate due to weak modulation depth.

Concerning the DFB-FL Gaussian profile, it needs a larger length but weaker modulation depth to give a narrower FWHM, smaller reflectivity, and smaller SLSR than the Gaussian apodized FBG, as shown in Table 2. This makes the Gaussian FBG filter preferable in filtering applications.

The DFB-FL Cauchy profile needs a smaller length, weaker modulation depth to give a smaller peak reflectivity, wider FWHM (0.54 nm) and suppressed side lobes compared to the Cauchy apodized FBG, but the

Table 2. Some apodized FBG profiles used as a filter.

Apodization profile	L (mm)	n_o	FWHM (nm)	Peak reflectivity	SLSR (dB)	Note	Ref. no.
Gaussian	10	2×10^{-4}	0.16	0.915	18	with side lobe	[8]
Positive-tanh	100	10^{-5}	0.2	0.999	–	no side lobe	[16]
Uniform	10	10^{-4}	0.15	0.92	8	with side lobe	[21]
Raised cosine	30	2×10^{-4}	0.18	1	–	no side lobe	[21]
Tanh	100	0.77	0.06	1	1.5	with side lobe	[22]
Hamming	100	0.77	0.02	0.75	9	with side lobe	[22]
Cauchy	100	0.77	0.03	1	2.6	with side lobe	[22]
Blackman	100	10^{-3}	0.04	0.92	–	no side lobe	[26]
Triangular spectrum FBG	100	2.27×10^{-4}	6	0.8	–	no side lobe	[27]
Triangular FBG with asymmetrical spectrum	2	5×10^{-4}	1	1	–	no side lobe	[28]
Raised cosine	45	10^{-4}	0.1	0.999	–	no side lobe	[25]
Inverse Gaussian	8	4×10^{-4}	0.2	0.9958	4.5	with side lobe	[29]

existence of side lobes in the Cauchy apodized FBG make the DFB-FL the better design between the two.

Generally, this work shows that careful choice of apodized DFB-FLs can provide optical filters with weaker modulation depths, smaller grating length, higher reflectivities, higher SLSRs, and narrower FWHM than those designed using the apodized FBGs.

4. Conclusion

This work has explored the viability of using the DFB-FL as an accurate C-band optical filter; changing the apodization profile will affect the filter performance. The best performance can be achieved by proper selection of both the grating length and modulation depth through the active grating region. This can be used to increase the flexibility in choosing optical filters according to WDM system filtering requirements.

Considering UDWDM filter applications, no apodization profile achieves the all-optical filter requirements stated previously. A tradeoff should be made in choosing the most suitable apodization according to system requirements. Generally, this work suggests DFB-FLs with a positive-tanh apodization profile as the best apodization profile with grating length (L = 25 mm) and modulation depth ($n_o = 10^{-5}$) as the most suitable filter for UDWDM filtering specifications among famous FBG profiles as well as the apodized DFB-FLs under consideration. This choice provides a FWHM of 0.048 nm, suppressed side lobes, and peak reflectivity of 1.906.

References

[1] Newton, S.A.; Jackson, K.P.; Moslehi, B.; Tur, M.; Cutler, C.C.; Goodman, J.W.; Shaw, H.J. *IEEE Trans Microwave Theory Tech.* **1985,** *33* (8), 193–210.

[2] Song, T.-T.; Zhao, Y.; Huo, Z.-W. *J. Lightwave Technol.* **2011,** *29*, 3672–3675.

[3] Iezekiel, S.; Cusick, T.A.; Miles, R.E.; Sales, S.; Capmany, J. *IEEE Trans. Microwave Theory Tech.* **1997,** *45* (8), 1458–1462.

[4] Johns, S.; Norton, D.; Keefer, C.; Soref, R. *IEEE Photonics Technol. Lett.* **1994,** *6*, 831–832.

[5] Vidal, B.; Polo, V.; Corral, J.L.; Marti, J. *IEEE Photonics Technol. Lett.* **2003,** *15*, 584–586.

[6] Zeng, F.; Yao, J. *J. Lightwave Technol.* **2005,** *23*, 1410–1418.

[7] Louis, H.; Amr, N.; Duncan, M.F.; Viswanath, R. *J. Opt. Soc. Am. A* **2009,** *26* (8), A1–A10.

[8] Najjar, M.; Ferchichi, M.; Rezig, H. In *Proceedings of the IEEE International Conference on Transparent Optical Networks "Mediterranean Winter"*, Marrakech, Morocco, Dec 11–13, 2008**;** IEEE: Washington, DC, 2008.

[9] ITU-T. In *Spectral Grids for WDM Applications: DWDM Frequency Grid*; International Telecommunication Union: Geneva, Switzerland, 2012; pp G.680–G.699.

[10] Najjar, M.; Ferchichi, M.; Rezig, H. In *Proceedings of the 17th IEEE International Conference on Telecommunications (ICT)*, Doha, Qatar, Apr 4–7, 2010**;** IEEE: Washington, DC, 2010.

[11] Ugale, S.; Mishra, V. *Int. J. Eng. Sci. Technol.* **2010,** *2*, 4463–4468.

[12] Ennser, K.; Zervas, M.N.; Laming, R.I. In *Proceedings of the 22nd European Conference Optical Communications (ECOC 96)*, Oslo, Norway, Sept 19, 1996**;** IEEE: Washington, DC, 1996.

[13] Varming, P.; Kristensen, M.; Hübner, J. *Electron Lett.* **1997,** *33*, 139–140.

[14] Wonga, A.C.L.; Chungb, W.H.; Tamb, H.Y.; Lua, C. *Laser Phys.* **2011,** *21*, 163–168.

[15] Wang, Q.; Zhao, Y.; Chang, J.; Ni, J.; Wang, Z. In *Proceedings of the International Conference on Electronics and Optoelectronics (ICEOE 2011)*, Dalian, Liaoning, China, Jul 29–31, 2011**;** IEEE: Washington, DC, 2011.

[16] Zervas, M.N.; Ennser, K.; Laming, R.I. *IEEE J. Quantum Electron.* **1998,** *34*, 770–778.

[17] Scifres, D.R.; Streifer, W.; Burnham, R.D. *IEEE J. Quantum Electron.* **1977,** *13*, 134–141.

[18] Low, A.L.Y.; Lim, K.Y.; Chien, S.F.; Ghafouri-Shiraz, H. *IEEE J. Sel. Top. Quantum Electron.* **2005,** *11*, 913–918.

[19] Sen, D.; Azmi, A.I.; Peng, G.D. *Proc. SPIE* **2009,** *7386*, 73860K.
[20] Hamdallah, T.A.; Mahran, O.; Aly, M.H.; El-Samahy, A.E. *J. Appl. Sci. Res.* **2009,** *5*, 1604–1610.
[21] Erdogan, T. *J. Lightwave Technol.* **1997,** *15*, 1277–1294.
[22] Shermin, S.; Khan, A.; Islam, M.S. *J. Commun.* **2012,** *7*, 840–846.
[23] Pastor, D.; Capmany, J.; Ortega, D.; Tatay, V.; Marti, J. *J. Lightwave Technol.* **1996,** *14*, 2581–2588.
[24] Gonze, D.; Gillespie, D.T. *Numerical Methods to Solve Ordinary Differential Equations*, 2009, http://homepages.ulb.ac.be/~dgonze/TEACHING/numerics.pdf (accessed Sep 2, 2013).
[25] Hedara, R.; Ikhlef, A.; Chikh-bled, M. *Int. J. Comput. Sci. Issues* **2012,** *9*, 368–374.
[26] Tamura, K.; Komukai, T.; Nakazawa, M. *IEEE Photonics Technol. Lett.* **1997,** *9*, 934–936.
[27] Feng, D.; Lv, M.; Yang, D. In *Proceedings of the Conference on Lasers & Electro-Optics & The Pacific Rim Conference on Lasers and Electro-Optics (CLEO/PACIFIC RIM '09)*, Shanghai, Aug 30–31, 2009**;** IEEE: Washington, DC, 2009.
[28] Wen, C.-K.; Chen, J.-C.; Ting, P. *IEEE Photonics Technol. Lett.* **2013,** *25*, 295–298.
[29] Welehtsan, M.N.; Padhy, B.B. *J. Emerging Trends Eng. Appl. Sci.* **2011,** *2*, 921–924.